## Work Package 3: What are the reasons for trends in the upper troposphere and lower stratosphere of chemical compounds relevant for climate change?

## Contribution of FZ J (LAVERO)

The major aim of this work package was the study of stratospheric und upper tropospheric chemistry, to investigate possible reasons for observed trends of chemical compounds relevant for climate change. Within the framework of this project, the contribution of FZ Jülich was mainly concentrated on the investigation of real winter episodes and the comparison between observations and model results. For this purpose the **C**hemical **La**grangian **M**odel of the **S**tratosphere CLaMS (McKenna, 2001a and b) which has been developed at FZ Jülich was improved and extended to enable the model to run long term three-dimensional simulations which are necessary to quantify the changes in budgets of stratospheric constituents. The first improvement made in the beginning of the project was the extension of the mixing module to three dimensions thus allowing for simulations of cold winter episodes with strong vertical downward motion inside the vortex (see Konopka et al., 2004). Since the module was in the state of testing at that time, the first study on the depletion of stratospheric ozone for this project was carried out with the two-dimensional version of the model. This was justified partly because of the fact that the winter 1999/2000 was not very cold, thus only showing slow descent rates inside the arctic polar vortex.

The simulations were carried out for the Northern hemisphere on 4 isentropic levels between 400 K and 475 K. The initialisation for early February was based on observations obtained by satellite (HALOE, POAM-3), balloon (Triple) or aircraft (ER-2), if possible. For some constituents tracer/tracer correlations were used, in other cases we used results from the Mainz 2d model mapped onto equivalent latitudes. Some data used for initialisation are shown in Figure WP3-1.

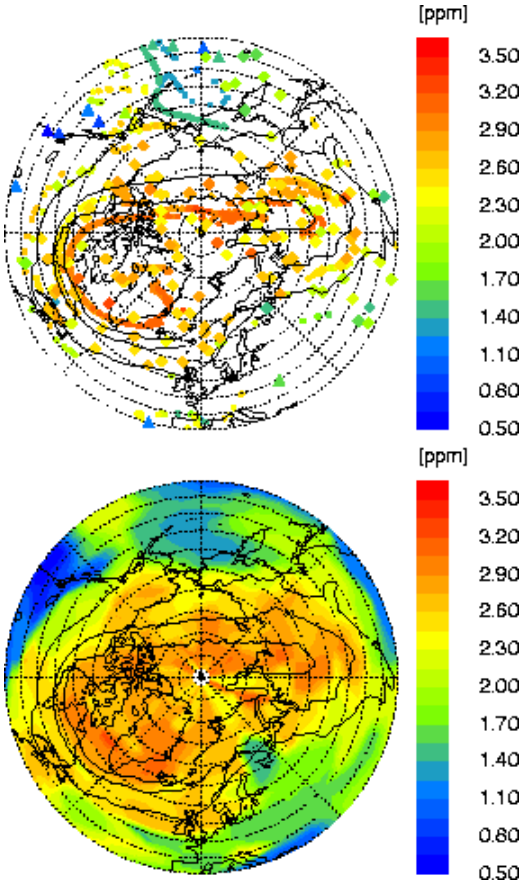


**Figure WP3-1:** Ozone initialisation on 450 K for February 10, 2000. The upper panel shows the locations of air parcels measured by ER-2 (circles), POAM (diamonds) and HALOE (triangles) mapped onto a synoptic date. The CLaMS initialisation derived from these data are shown in the lower panel.

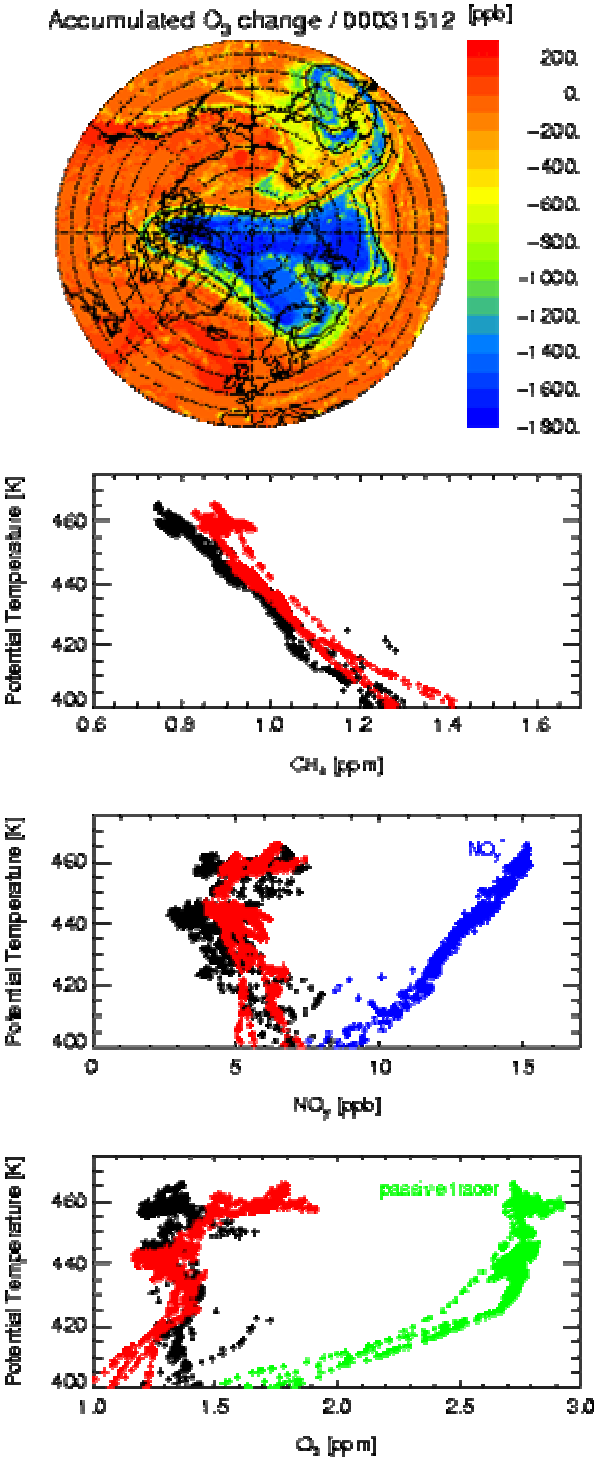


**Figure WP3-2:** Results from an isentropic CLaMS simulation for spring 2000: accumulated ozone change in ppb on 450 K for March 15th, 2000 (upper panel); comparison between ER-2 observations (black) and model results (red) for the flight on March 12th (lower panel). NOy* without denitrification (see text).

Since significant denitrification has been observed, a parameterisation for this process based on $NO_y$ and $N_2O$ observations made on board the ER-2 and the temperature history of the air masses considered was introduced into the model. The results concerning denitrification and ozone loss are shown in Figure WP3-2. A three-dimensional version of CLaMS has been developed to allow longer simulations for several months under realistic conditions. The results of first runs without chemistry utilising ozone and methane observations obtained by OMS and Triple are shown in Figure WP3-3. Comparisons between observed and simulated methane in December 1999 and March 2000 show that CLaMS is capable of simulating the descent inside the vortex quite well. A similar comparison concerning ozone allows to estimate the chemical ozone loss inside the vortex, with a resulting maximum loss of 60% in the lower stratosphere. To study mixing across the vortex edge an additional tracer was initialised on December 1st, 1999 with values of 1 inside the vortex and values of 0 outside.

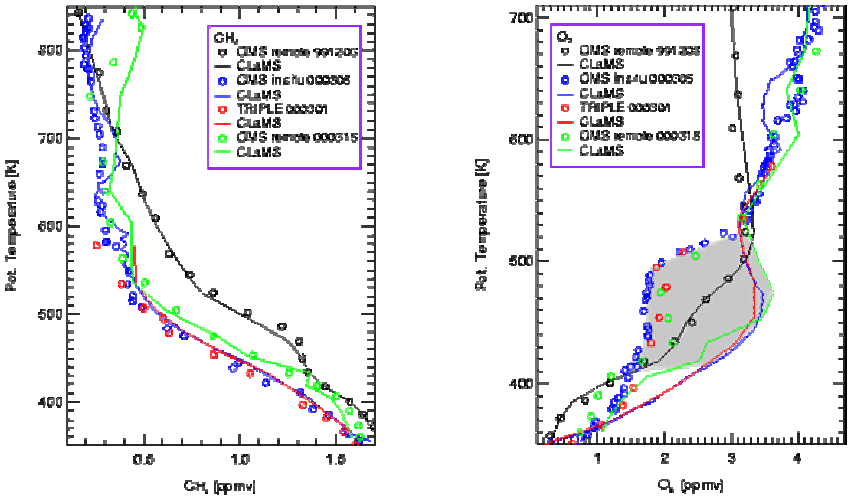


**Figure WP3-3:** Vertical profiles of methane (left) and ozone (right) obtained by observations (circles) in December 1999 and March 2000 compared to profiles derived from CLaMS simulations.

The distribution of this tracer describes the motion and composition of the vortex air. Mixing strongly influences the composition of the vortex in December when the vortex edge is still formed, while large scale intrusions, coinciding with enhanced planetary wave activity, occur later in January (see Figure WP3-4). The vortex remained well-isolated until mid of March in the altitude range 500-600 K.

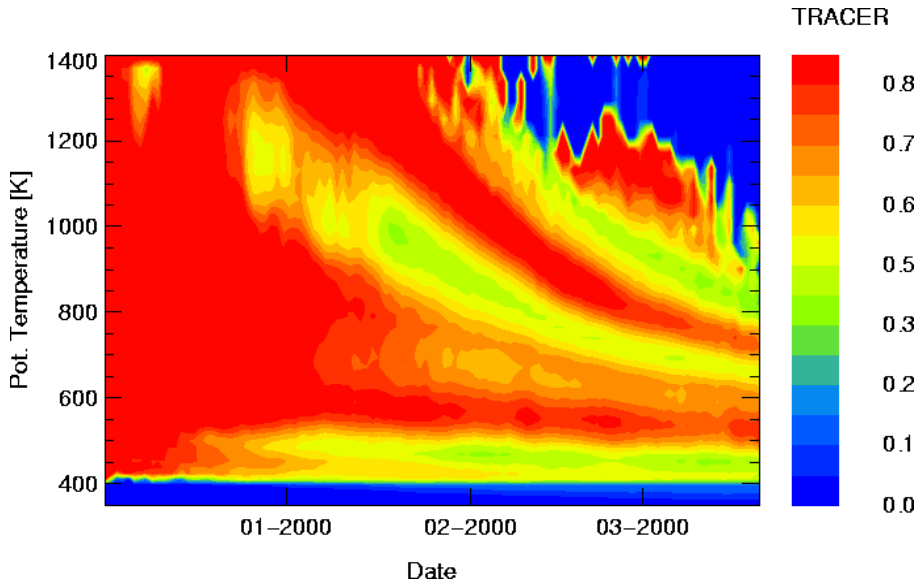


**Figure WP3-4:** Temporal evolution of the vortex averaged tracer (see text). The vortex edge was defined using the Nash criterion.

For more information about the simulations of this arctic winter see Grooß et al. (2002) and Konopka et al. (2003).

In the framework of estimation of climate relevant tracers further studies concerning the isolation of the polar vortex and its chemistry based on the winter 2002/2003 have been carried out. The polar vortex of this winter was heavily disturbed by planetary waves. After having been split into two lobes during mid January 2002, a re-merge of the vortex was observed a few days later. Besides causing vigorous mixing in the vicinity of the vortex edge the repeatedly splitting, folding and re-merging lead to strong filamentation of the interior of the lower stratospheric vortex with mid latitudinal air masses being folded into the vortex.

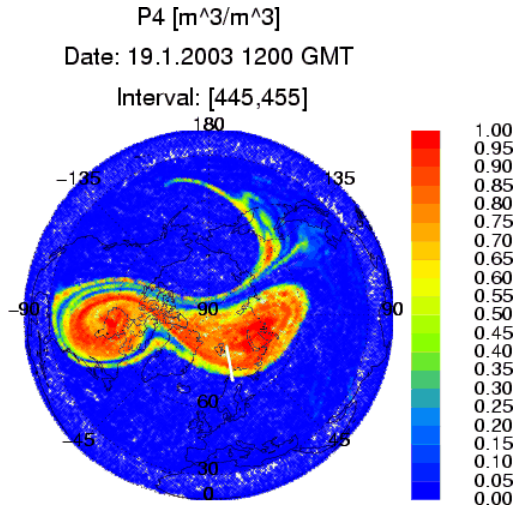


**Figure WP3-5:** Horizontal distribution of the tracer P4, marking the interior of the vortex core, on the 450 K isentropic level for January 19th , 2003.

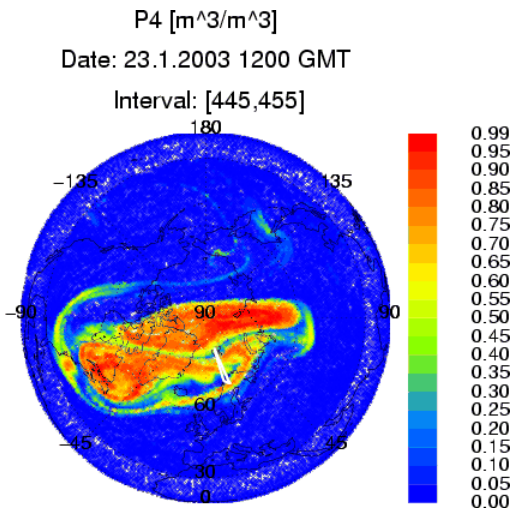


**Figure WP3-6:** Horizontal distribution of the tracer P4, marking the interior of the vortex core, on the 450 K isentropic level for January 23rd , 2003.

Both, the effects of the mixing at the vortex edge and the transport of air masses from outside into the vortex are illustrated by the results of a CLaMS simulation utilising a suite of inert tracers tagging the original position of the air masses. The simulation was started on December 15th, 2002, with the inert tracers mentioned above initialised as shown in Table WP3-1. The PV used for initialisation has been modified to account for the strong vertical gradient of PV. The resulting modified PV (mPV) shows the same conservation properties as PV, but allows to defne height-independent values for the vortex edge (Müller and Günther, 2003). The horizontal and vertical resolution was 90 km and 8 K, respectively.

Figure WP3-5 shows the situation of the polar vortex on January 19th, 2003. The distribution of the inert tracer P4 on the 450 K isentropic level is shown symbolising air masses originating in the vortex core. Tracer values different from 1 and 0 show the effects of mixing. The vortex is strongly elongated, almost splitting into two secondary vortices. Distinct filaments of vortex air are wrapping around anticyclones being built up due to PV conservation.

On January 23rd the two vortices are about to re-merge, a thin filament of mid latitudinal air being trapped between them (see Fig. WP3-6). The mixing inside the newly formed vortex is small enough to let signatures of these air masses survive for several days. The tongue of vortex air moved to the mid latitudes observed on the 19th has been mixed into its environment to a large degree.

| ***Inert Tracer*** | ***mPV Range*** | ***Description*** |
|---|---|---|
| P0 | 0.,...,10. | Tropics |
| P1 | 10.,...,14. | Mid Latitudes |
| P2 | 14.,...18. | Outer Vortex Edge |
| P3 | 18.,...,21., | Inner Vortex Edge |
| P4 | ≥ 21. | Vortex Core |

**Table WP3-1:** Initialisation of the inert tracers according to the modified PV value at the positions of the air masses on December 15th, 2002.

The dynamics of the polar arctic stratosphere lead to enhanced transport in and out of the polar vortex (see Fig. WP3-7). The vortex interior showed signs of both enhanced and reduced mixing, depending

on the history of the air masses involved. Some parts of the lower stratospheric vortex showed a fraction of up to 50% air originating from the mid latitudes and the outer vortex edge. The total effect on the lowest part of the vortex is about 25%, but only 2% when the whole simulated vortex between 325 K and 600 K is considered. The effect of transport of vortex core air masses into the mid latitudes and their subsequent mixing into their environment is much larger. About 10% of the vortex mass is exchanged by horizontal transport and mixing, being substituted by vertical transport from the middle and upper stratosphere.

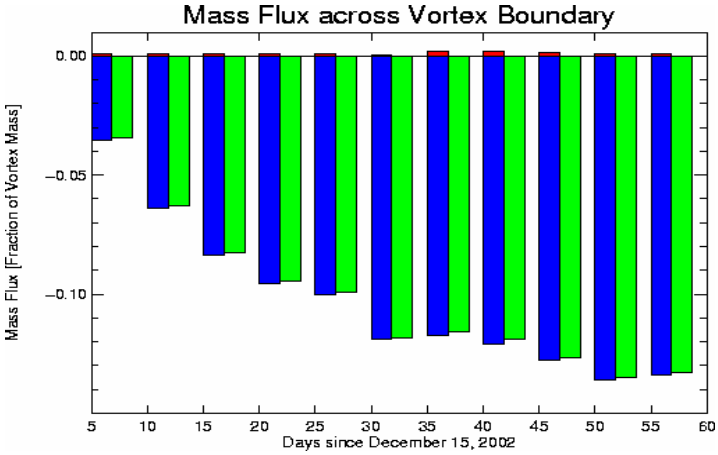


**Figure WP3-7:** Estimated accumulated cross-boundary flux in the region between 325 K and 600 K (i.e. the lower stratosphere) displayed as fraction of vortex mass derived from the air mass origin spectra for the CLaMS simulation. The flux into and out of the vortex is shown in red and blue, respectively. The net flux is shown in green. The vortex edge was computed from ECMWF data using a value of 21 mPVU. The calculation was carried out assuming a mean distance between the model air masses of 60 km. During the simulation the area of the vortex interior decreased by about 15%.

With the help of the spectra of air mass origins it is possible to give an estimate of the cross-boundary flux in the model atmosphere during the above mentioned simulation. This was carried out by integrating over the non-vortex parts of air masses inside and vortex originating parts of air masses outside the vortex defined by the 21 mPVU contour line (see Table WP3-1).

The model results show an increase in air mass exchange during December and the beginning of January. The outflow reaches values of about 13% of the total vortex mass of the considered height range. The highest influx values (about 2% of net flux) occur, when the vortex has almost split and extra-vortex air is trapped inside the vortex during the re-merge. The highest influxes are confined to the lowest part of the vortex, where the cross-boundary exchange is stronger due to stronger filamentation and enhanced mixing. The total influx reaches here approximately 25 % of the total vortex mass.

During this winter an European field campaign investigating the chemistry and dynamics of the arctic stratosphere took place. The measurements obtained gave clear evidence of re- and denitrification processes inside the polar vortex. Utilising the further developed CLaMS model these processes were simulated allowing for interpretation beyond the observations. The newest developments of the CLaMS model include an enhanced parameterisation for the development, transport and sedimentation of large NAT particles, the so-called 'NAT rocks', which are currently under suspicion to be responsible for the strong de- and renitrification processes sometimes observed inside the lower stratospheric vortex. Figure WP3-8 shows the temporal evolution of the deviation of the models $NO_y$ from $NO_y^*$ poleward of 65 degrees equivalent latitude, usually being a good indicator for re- and denitrification.

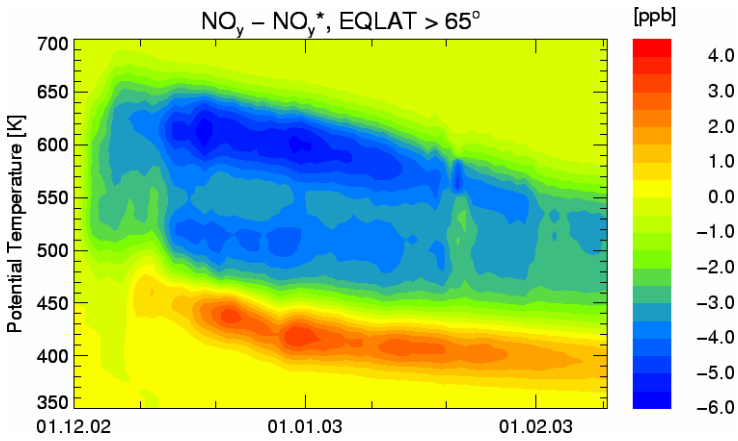


**Figure WP3-8:** Temporal evolution of the deviation of $NO_y$ from $NO_y^*$ poleward of 65° equivalent latitude.

In the mid of December 2002 the vortex interior is characterised by very low temperatures, allowing for the nucleation and growth of large NAT particles. Due to sedimentation these particles lead to a strong downward transport of nitrous oxygen. As they leave the cold regions in the lower stratosphere, they reach areas of subsaturation, where the nitrous oxygen is released back into the gas phase due to melting thus leading to renitrification.

The horizontal distribution of the above mentioned quantity on the 425 K isentropic surface (see Figure WP3-9) shows a strong inhomogeneity of de- and renitrifaction areas throughout the vortex interior. Air masses which have undergone these processes some time ago can be observed inside small filaments peeled off the vortex and moved into the mid latitudes, slowly mixing into their environment. The pink line corresponds to the flight path of the M-55 Geophysika, which carried out a mission that day. The measurements obtained during that flight are shown together with CLaMS results in Figure WP3-10. They are in general in good agreement with the observations, although CLaMS shows stronger denitrificaton on the higher flight level. This is possibly due to the patchy structure mentioned above and the comparatively coarse CLaMS resolution.

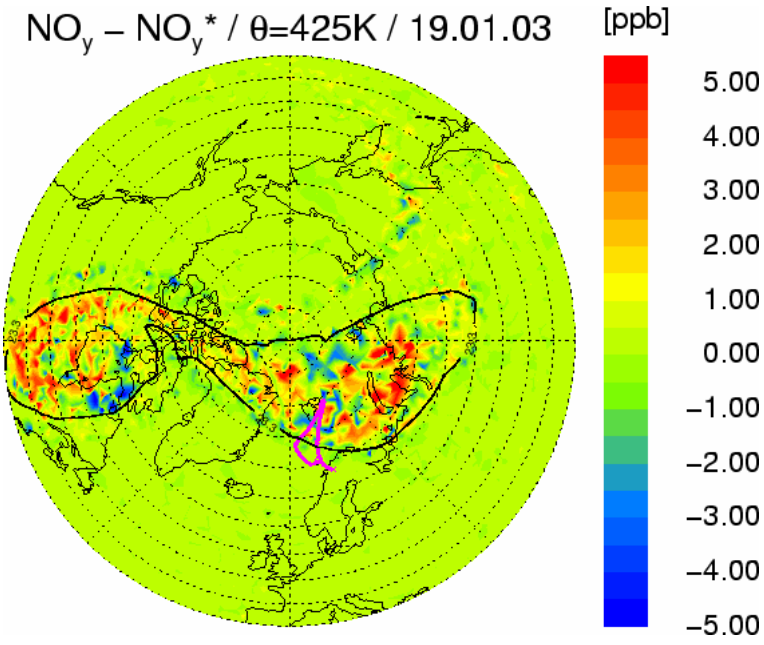


**Figure WP3-9:** Horizontal distribution of the deviation of $NO_y$ from $NO_y^*$ on the 475 K isentropic surface for January 19th, 2003. The thin black line denotes the vortex edge.

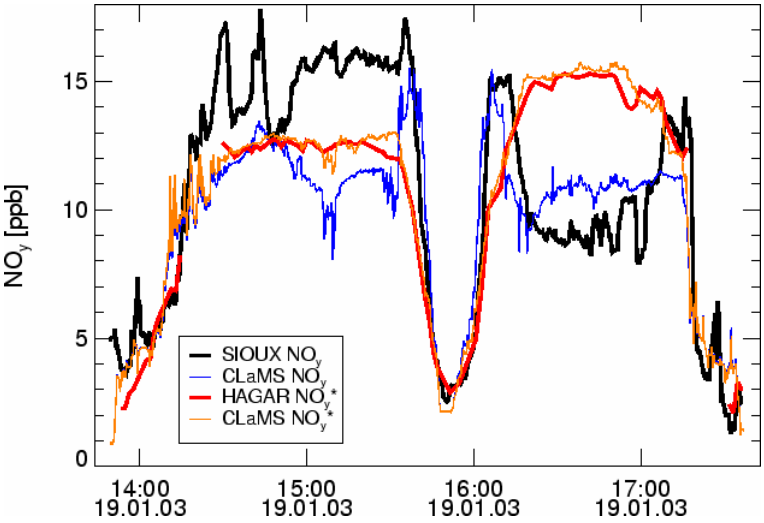


**Figure WP3-10:** Measurements of $NO_y$ and $NO_y^*$ obtained on the flight on January 19th , 2003, together with CLaMS results interpolated onto the flight path.

The ozone destruction derived from this simulation for the 500 K isentropic level is shown in Figure WP3-11. Ozone loss of up to 400 ppbv occurs in air masses inside the vortex. Again the inhomogeneity inside the polar vortex can be noticed. Ozone reduced air masses being peeled off the vortex edge and moved equatorward can be observed in the mid latitudes, forming filaments and small structures.

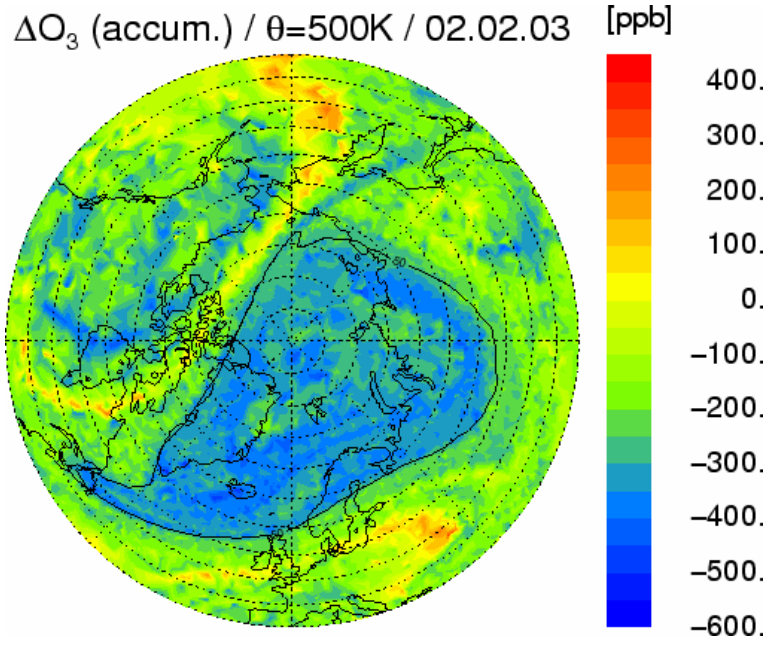


**Figure WP3-11:** Accumulated ozone loss on the 500 K isentropic surface for the 2nd of February, 2003. The thin black line denotes the vortex edge.

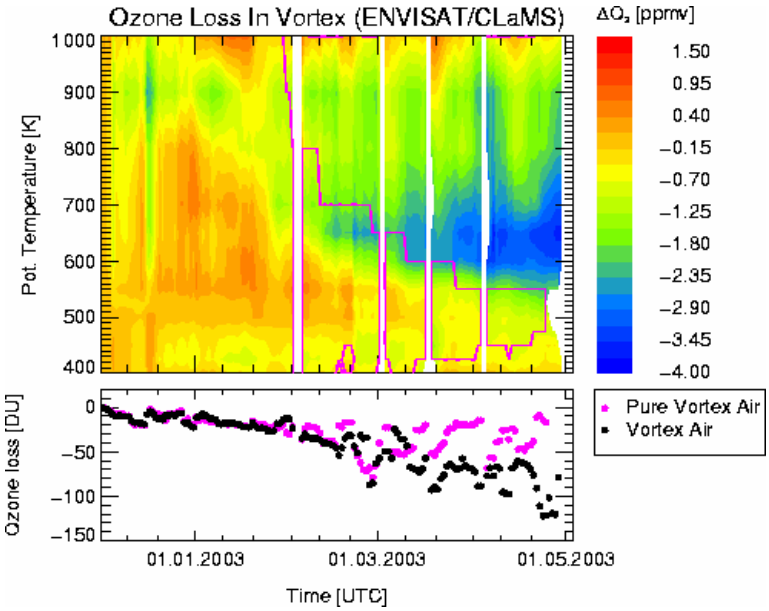


**Figure WP3-12:** Ozone loss as defined as difference between an inert tracer transported by CLaMS and observations derived from ENVISAT measurements. The lower panels shows the results in total ozone distinguishing between pure and mixed vortex air.

Another simulation has been carried out to investigate the total amount of ozone destruction as compared to observations. Figure WP3-12 shows the difference between ozone transported as an inert tracer by CLaMS and ozone derived from ENVISAT observations inside the vortex. The vortex is considered as all air masses with at least 80 % vortex air with respect to the beginning of the simulation, indicated by the purple line. Starting in December ozone loss can be observed already below 500 K. In the beginning of February strong ozone loss starts between 600 and 700 K. During this time the vortex undergoes strong dilution. The ozone loss increases up to 4 ppmv due to $NO_x$ chemistry. The lower panel of Figure WP3-12 shows the total ozone loss distinguishing between pure vortex air masses and air masses with mixed in mid latitude air. During the first part of winter no difference with respect to ozone loss can be found between these two types of air. In February and March mixed air shows considerably higher ozone loss then pure vortex air.

The simulations on several arctic winters carried out with CLaMS indicate substantial chemical disturbances in the lower arctic stratosphere, leading to (depending on the meteorological situation) more ore less enhanced ozone depletion over the northern hemisphere. The processes which are currently under suspicion of leading to the ozone destruction like chlorine activation by heterogeneous reactions on PSC surfaces, the occurrence and effects of NAT rocks (which formation processes are not yet understood), denoxification, de- and renitrification are represented very well in the model.

The results of the aforementioned simulations concerning the distribution and temporal evolution of trace constituents like ozone, nitrous oxide, water vapour etc. are supported by observations made in situ as well as by remote sensing instruments. Although not every process playing a role in stratospheric chemistry is well understood and its net effects quantified, the development of the model has reached a state, where it can be used as diagnostic as well as a prognostic tool for both, standalone winter simulations and as companion for field campaigns.

In the following chapters time-slice and transient simulations with CCMs forced at the lower and upper boundary are considered. This includes analysis of trends in chemically active gases and temperatures, but also changes and variability in lower stratospheric polar processes and comparisons with the previous chapter.

# Contribution from DLR

## Investigation of trends in the tropopause region derived from the chemistry-climate model E39/C

Among others, the data of the transient simulation (1960-1999) carried out with E39/C has been used to estimate the variability and long-term changes in the UT/LS with particular focus on the tropopause. The transient simulation, which was jointly defined with MPI-MAECHAM and MPI-C, considers the quasi-biennial oscillation (QBO), the 11-year solar activity cycle, and the large volcanic eruptions of Agung (1963), El Chichon (1982) and Pinatubo (1991). Changes of greenhouse gas concentrations ($CO_2$, $CH_4$, $N_2O$) and (natural and anthropogenic) emissions are considered according to observations. The sea surface temperatures (SSTs) are adopted from the Hadley Centre. (A complete description of the transient model simulations will be published very soon.) Here, some first results of this transient model simulation is presented, which impressively indicates the potential of this simulation for further analyses, in particular with respect to observations. Additional results can be found in this report, see WPs 1, 4, 5, and 6.

Figure WP3-13 shows a comparison of global mean temperature anomalies derived from MSU Channel 4 (lower stratosphere, 13-21 km; 1979-2002) and corresponding results received from the E39/C transient simulation. The most obvious features are certainly the temperature increases immediately after the eruptions of Agung, El Chichon, and Mt. Pinatubo. It is evident that the temperature signals after the eruptions of El Chichon and Mt. Pinatubo are significantly larger than observed. The obvious explanation would be that the prescribed additional net-heating rates, which are adopted from Kirchner et al. (1999) for the post-Pinatubo phase and which are extrapolated from these for the two other eruptions, are too large. In any case, the temperature perturbation lasted only for about 3 years. Figure WP3-13 indicates that the modelled temperature trend is in good agreement with the MSU analysis. Interestingly, similar to the changes derived from MSU data, the model results also indicate stepwise changes towards lower temperatures in the lower stratosphere after the eruptions of El Chichon and Mt. Pinatubo, which is not simulated after the eruption of Agung. No obvious temperature trend is found in the years after El Chichon and Pinatubo, neither in MSU analysis nor in E39/C data. Looking more carefully to the modelled temperature anomalies, in particular to the year between 1965 and 1982, the QBO signal can be detected (see also WP6).

In the following changes at the thermal tropopause have been estimated from data derived from the E39/C transient model simulation. The changes of the pressure of the thermal tropopause are given in figure WP3-14. Whereas no obvious systematic changes (trends) are seen in the first two decades of the transient simulation, model results indicate a continuous change in tropopause height in subsequent years. In both hemispheres, E39/C simulates a decrease (increase) of tropopause pressure (height) poleward of around 50°. The subtropical regions show an increase (decrease) of tropopause pressure (height). No long-term changes can be detected in the tropics. The major volcanic eruptions considered in the transient simulation lead to a temporary increase of tropopause pressure. Changes in tropopause temperature (not shown) are directly related to the variability of the tropopause height: an increase (decrease) of tropopause height goes along with a decease (increase) of tropopause temperature. A comparison with an analysis of tropopause height changes at 47°N (e.g. Steinbrecht et al., 2001) shows a qualitative agreement, i.e. a more or less steadily increase of tropopause height in February during the last 30 years. However, here the model is underestimating the rise in tropopause height. The analysis of Steinbrecht and colleagues (2001) gives +125 m/decade for the station at Hohenpeissenberg, E39/C calculates +80 m/decade for the corresponding model grid point.

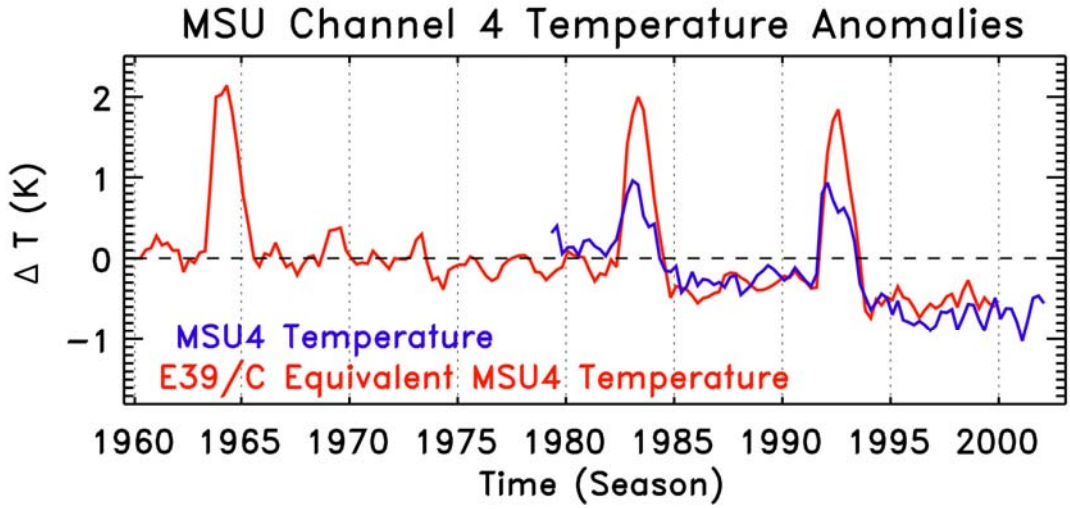


**Figure WP3-13:** Anomalies of global mean temperature (with respect to the years from 1979 to 1990) derived from MSU Channel 4 (lower stratosphere) and corresponding values derived from E39/C simulation.

Figure WP3-15 depicts the changes of water vapour mixing ratio at the thermal tropopause during the 40 year model simulation. The clearest indication for a change is only found in the subtropical regions, where the water vapour mixing ratios are obviously higher in the late 1980s and the 1990s. Systematic mutations in model results cannot be identified in the tropics and middle and high latitudes of both hemispheres. Again, the volcanic eruptions involve characteristic signatures (see WP6). Looking higher up into the lower stratosphere, a comparison with measurements of the Boulder frost point hygometer and corresponding HALOE data (Randel et al., 2004) is performed. The general distribution of the change pattern in the lower stratosphere is equal to that at the tropopause. The temporal development of water vapour changes at 40°N, 80 hPa in E39/C (not shown) indicates a similar increase in water vapour mixing ratio as shown by Randel et al. (their figure 8a). Looking at the changes detected in Boulder since 1980, an increase of approximately 1 ppmv is observed in 17 to 22 km until the year 2000. E39/C simulates an increase of about 0.7 ppmv at 80 hPa for the same time period.

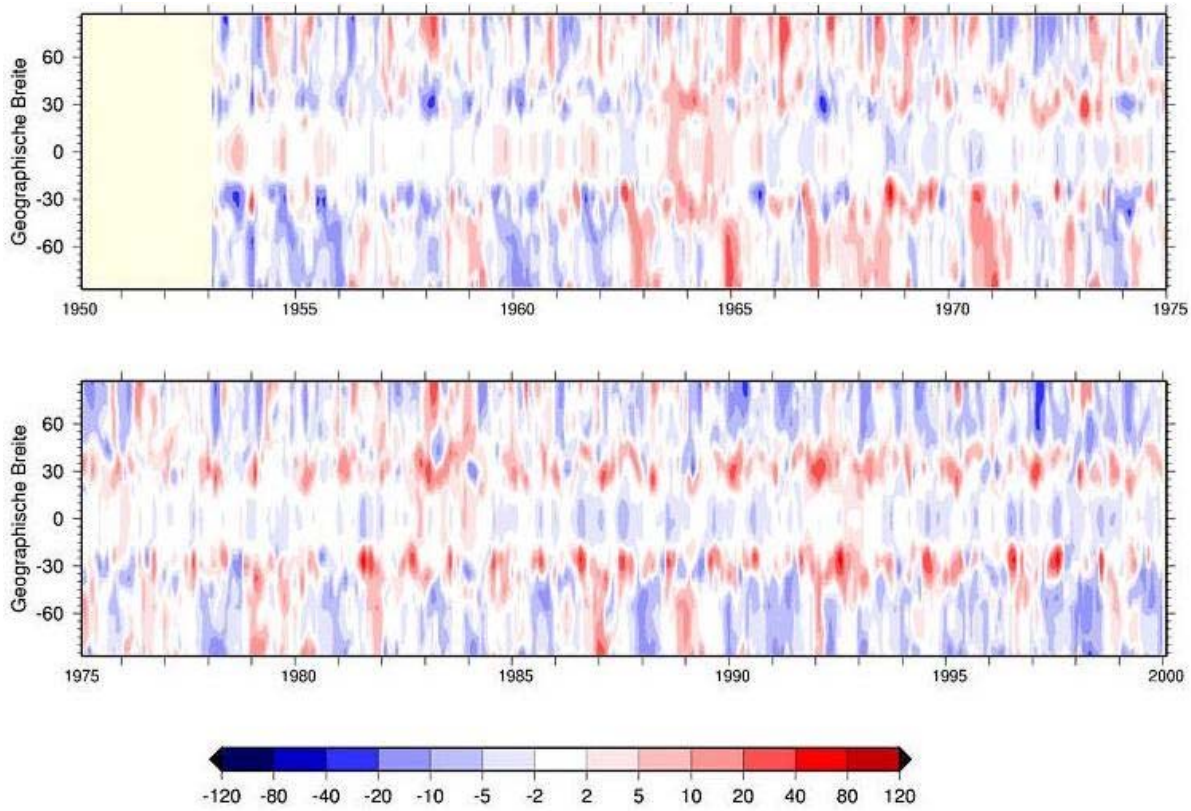


**Figure WP3-14:** Anomalies of tropopause pressure (in hPa) with regards to the model years 1960 to 1980.

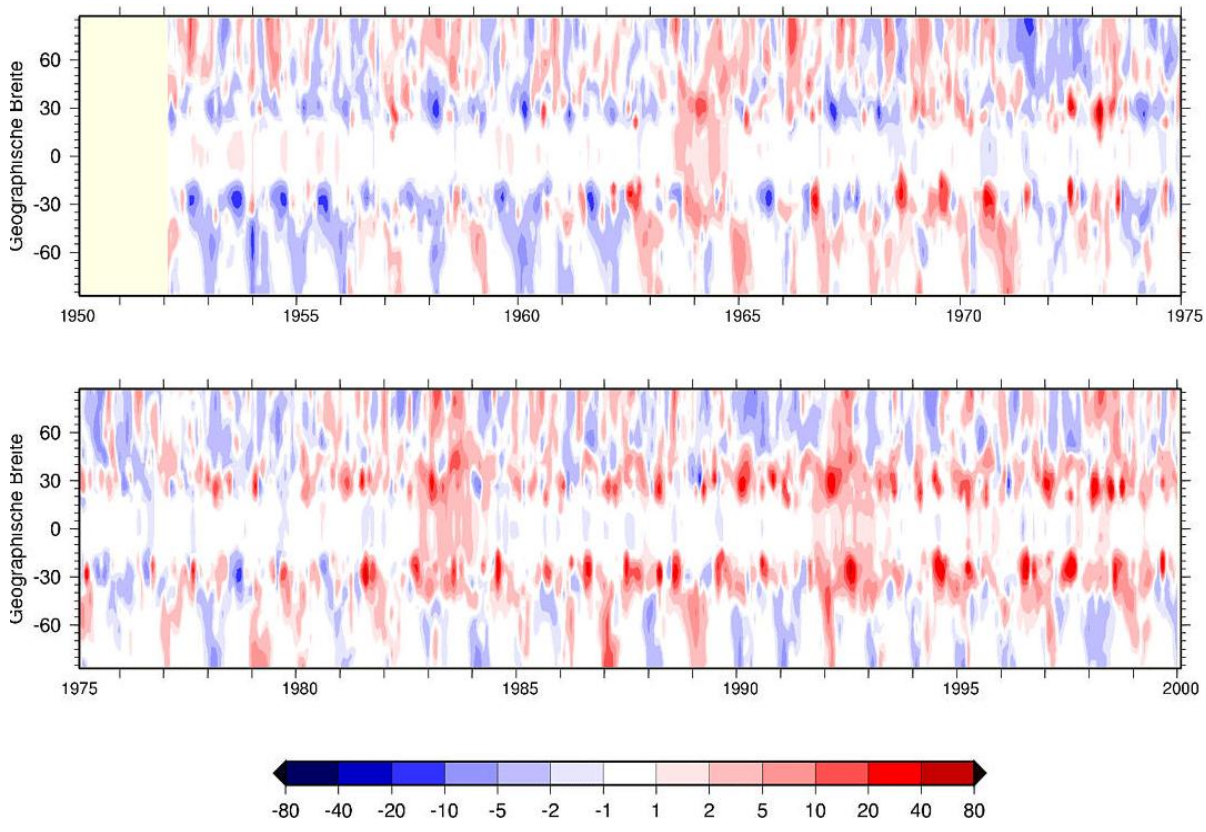


**Figure WP3-15:** Anomalies of tropopause water vapour mixing ratios (in ppmv) with regards to the model years 1960 to 1980.

## Joint contribution of MPI-C, MPI-MAECHAM and DLR

## 20 year timeslice experiments for the present (1990, 2000) and the near past (1960, 1980)

The simulations with the chemical GCMs MA-ECHAM/CHEM and E39/C (*Hein et al*, 2001) with fixed (seasonal) boundary conditions over 20 years are included already in an international comparison (*Austin et al*, 2003). Comparisons of temperature and ozone trends for MA-ECHAM-CHEM against observations are published in *Manzini et a*l, 2003. An important conclusion there is that feedback-processes between stratospheric chemistry and dynamics of the middle atmosphere are important for simulation of the observed cooling of the polar lower stratosphere in the late nineties and that changes in heating by descent can mask changes due to radiation (see also interim reports, a paper on predictions and sensitivity studies is in preparation).

## 40 year transient simulations with interactive CCMs

The transient simulations with MAECHAM4/CHEM and E39/C include forcings by greenhouse gases and chemically active gases, observed sea surface temperature (SST), major volcanoes (see previous chapter) and solar cycle. The quasi-biannual oscillation of the zonal wind in the lower tropical stratosphere (QBO) is assimilated from observations (*Giorgetta* and *Bengtson*, 1999). We found that inclusion of QBO is essential for the vertical tracer transport into the middle and upper stratosphere (presented at EGU, Nice 2004). The ElNino/LaNina signal in SST has a clear impact on stratospheric water vapour and ozone via tropical tropopause temperature in agreement with observations.

The 'tropical tape recorder' for the seasonal signal of stratospheric water vapour (Figure WP3-16) is well reproduced but slightly too fast (see also *Steil et al*, 2003). The figure shows the water vapour increase due to methane increase in the middle stratosphere in periods not perturbed by volcanoes. The volcanoes enhance stratospheric water vapour via heating of the 'cold point' (Figures WP3-17, WP3-19), causing more ozone destruction in the gas phase especially in the tropics (Figure WP3-16 to WP3-20). They lead also to a reduced ozone production via the 'photochemical smog reactions' in the lower stratosphere because of heterogeneous $NO_x$ depletion. A detailed analysis of all these natural effects on ozone and temperature was done together with DWD Hohenpeißenberg (see WP1), addition al results are in chapter WP6. In the tropics the features in the temperature and ozone changes of the lower stratosphere are rather similar for the two CCMs. In high latitudes the inter-annual variability is much larger in MA-ECHAM-CHEM related to feedbacks involving forcing from above, however a lot of inter-annual features appear also in E39/C which includes only forcing from below.

The chlorine increase due to the CFC-increase (simulated from the observed increase in CFC concentrations at the surface in MAECHAM4/CHEM) causes the downward trend of ozone in the upper stratosphere (Figure WP3-21) accompanied by a cooling (Figure WP3-22), the development of the Antarctic ozone hole in the early 80s (Figures WP3-18 and WP3-20) and ozone depletion in the arctic lower stratosphere. The patterns of ozone change at 70hPa are similar in total ozone changes. The models are even able, to reproduce some of the observed inter-annual variability in Antarctic and Arctic spring, including the offset of the vortex from the pole. A comparison of MAECHAM4/CHEM results with observed chemical ozone destruction (*Rex et al*, 2004) for the years 1992 to 1998 has been presented at EGU, Nice, 2004, Figure WP3-24 shows an example for a cold winter/spring. Figure WP3-23 shows corresponding results for Antarctica. If the same analysis is done for the sixties, only a slight chemical ozone destruction related to nitrogen chemistry is calculated for spring. Comparing with CLAMS, the simulation of denitrification and polar heterogeneous chemistry is less sophisticated (*Steil et al*, 2003), but nevertheless calculated ozone depletion is within observational uncertainty.

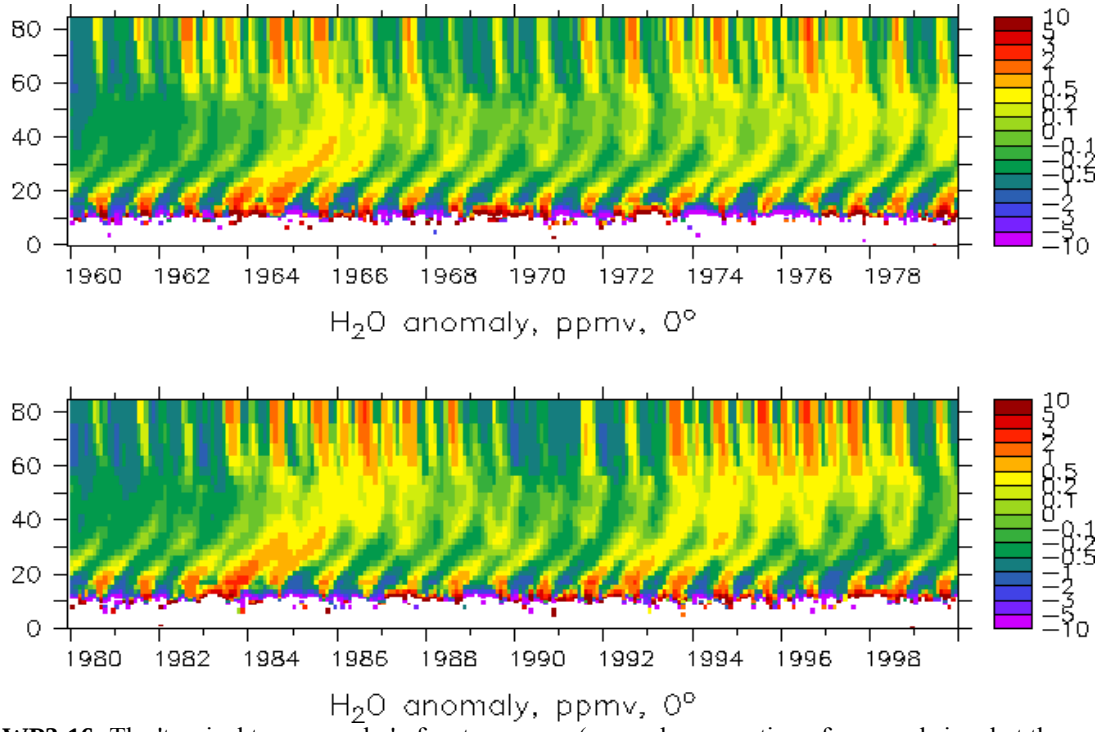


**Figure WP3-16:** The 'tropical tape recorder' of water vapour (upward propagation of seasonal signal at the tropopause) as calculated by MAECHAM4/CHEM. Note the increasing trend in upper stratosphere (in periods unperturbed by volcanoes) due to methane increase.

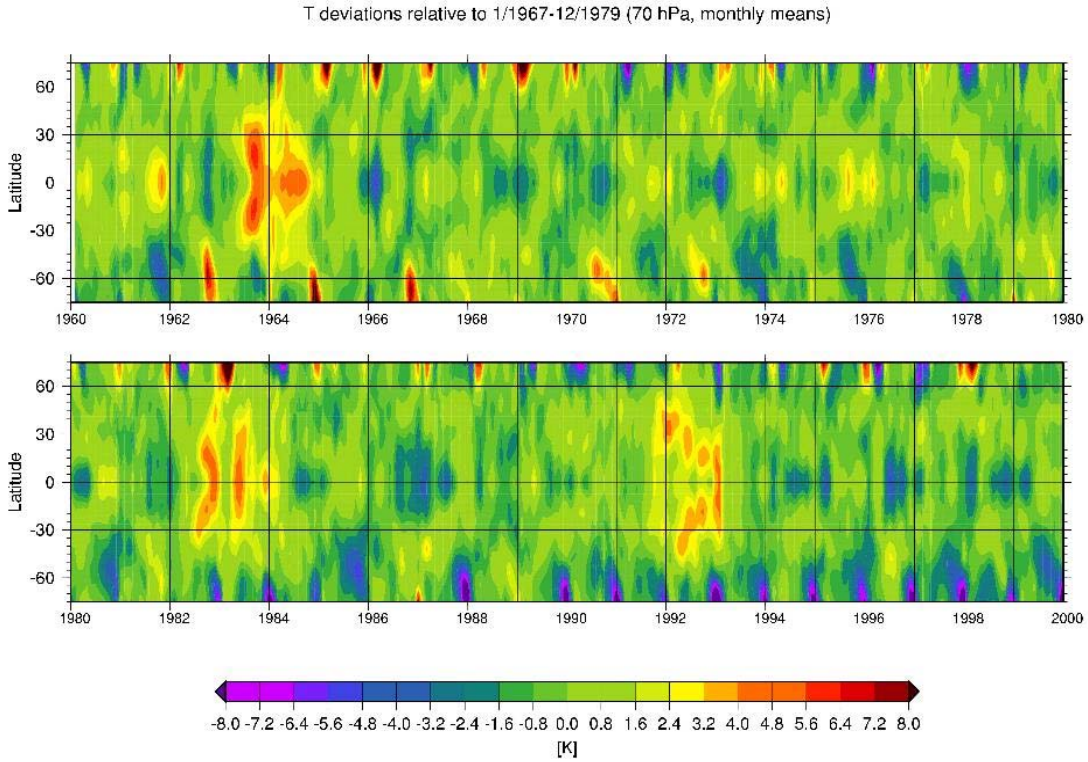


**Figure WP3-17:** Temperature deviations and trends calculated by E39/C at 70hPa, monthly zonal means, average seasonal cycle of 1967-1979 subtracted, peaks in tropics due to eruptions of Agung, El Chichon and Pinatubo.

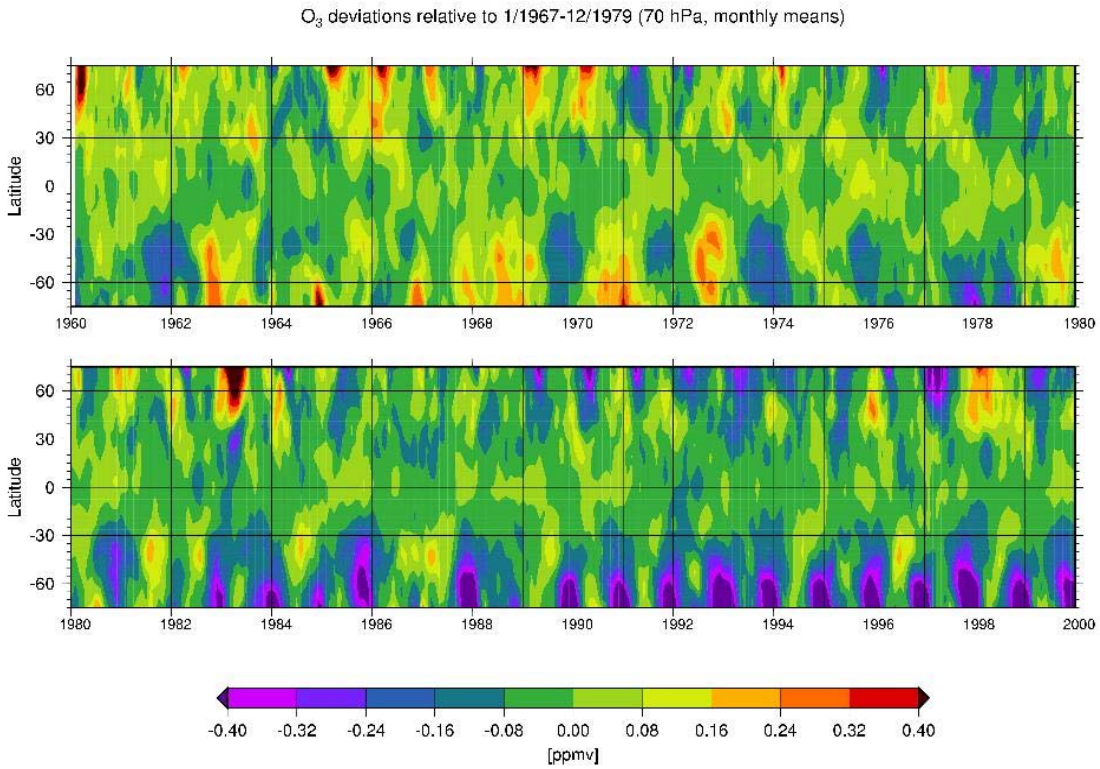


**Figure WP3-18:** Ozone deviations and trends calculated by E39/C at 70hPa, monthly zonal means, average seasonal cycle of 1967-1979 subtracted.

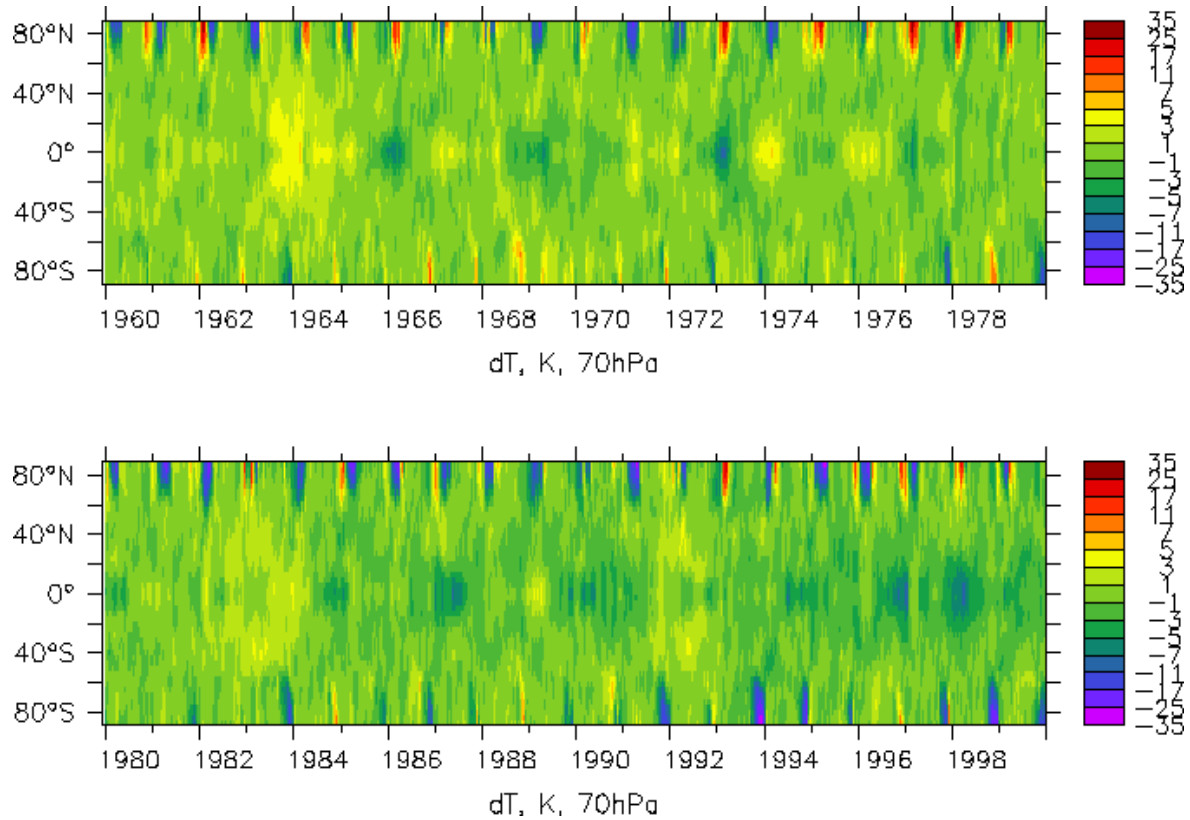


**Figure WP3-19:** As Figure WP3-17, but calculated with MAECHAM4/CHEM based on 10-day means, 1960-1979 subtracted.

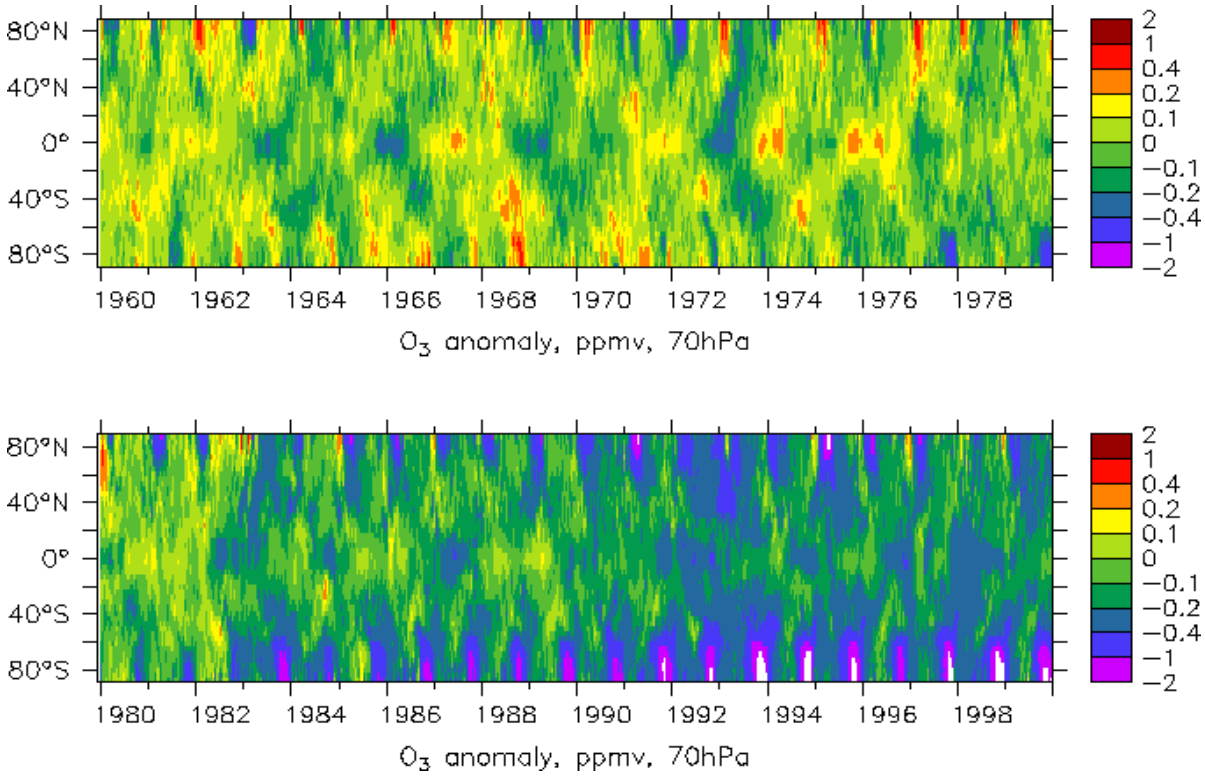


**Figure WP3-20:** As figure WP3-18 but calculated with MAECHAM4/CHEM based on 10day means, 1960-1979 subtracted. Note that the shorter averaging period causes a larger variability than in Figure WP3-18.

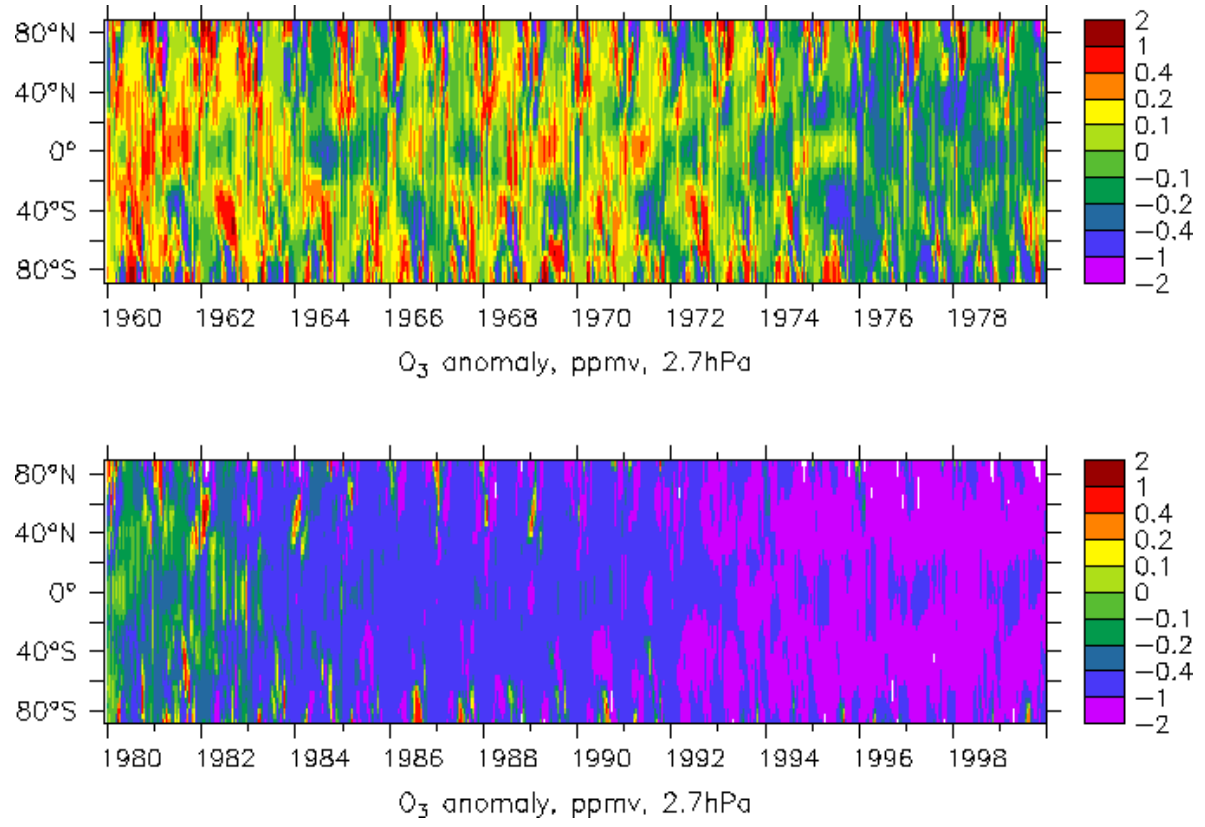


**Figure WP3-21:** Ozone changes and inter-annual variability at 40km calculated with MAECHAM4/CHEM (as Figure WP3-20). This altitude shows maximum changes due to homogeneous depletion by CFCs.

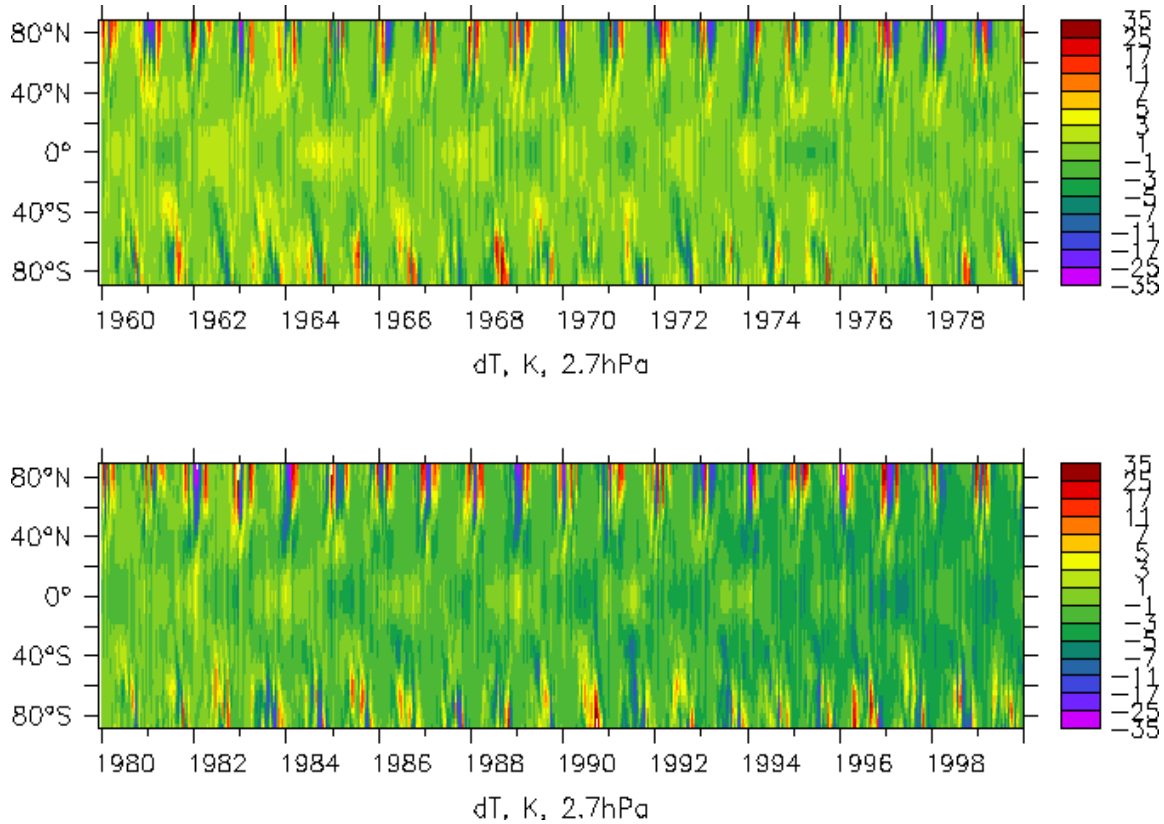


**Figure WP3-22:** Temperature changes and inter-annual variability at 40km calculated with MAECHAM4/CHEM. The cooling in the nineties is related to less absorption of solar radiation by ozone depletion and increased infrared emission by $CO_2$.

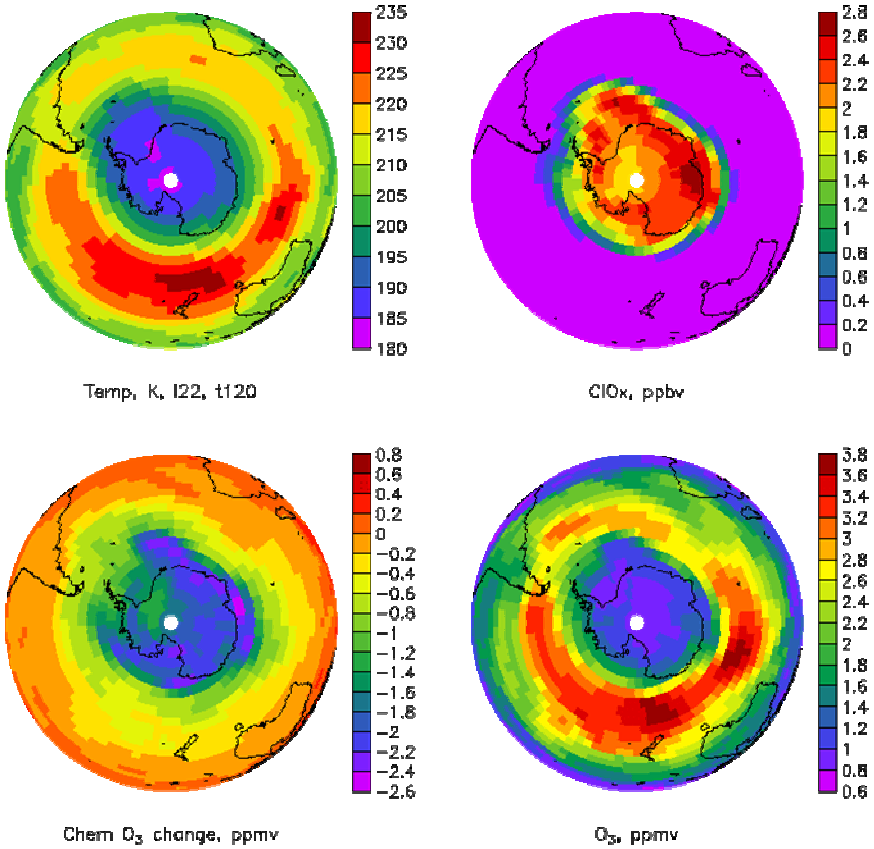


**Figure WP3-23:** Calculated temperature, active chlorine, chemical ozone destruction (using a passive ozone tracer) and ozone at 70hPa for Sept. 30, 1998, Antarctic with MAECHAM4/CHEM.

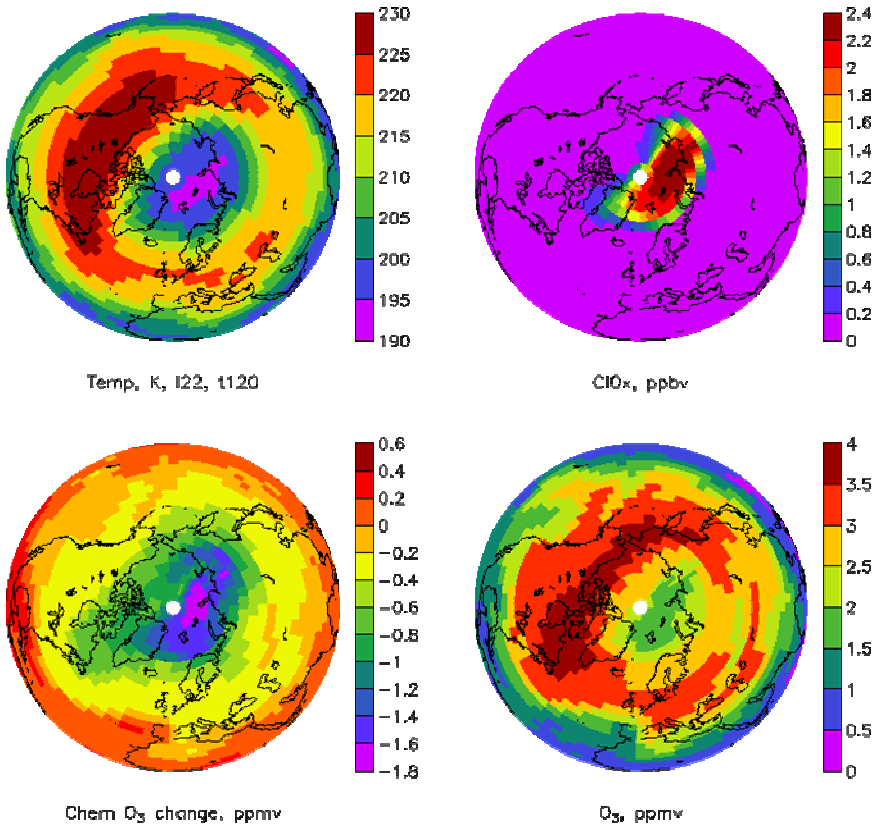


**Figure WP3-24:** Calculated temperature, active chlorine , chemical ozone destruction (using a passive ozone tracer) and ozone at 70hPa for March 30, 1996, Arctic with MAECHAM4/CHEM.

## Joint contribution by MPI-MIPS and MPI-C:

### Improvement of PSC parameterisation

The work is still in progress due to shortages in manpower and changes in model versions (ECHAM4 to ECHAM5). The coupling of SAM with the new Mainz PSC-scheme will be finished in the framework of the European project SCOUT. For the overall results on Arctic ozone depletion a new scheme would cause only subtle changes as discussed in *Steil et al.* (2003).

## New publications with contributions from WP3


Austin, J., D. Shindell, S. R. Beagley, C.Brühl, M. Dameris, E. Manzini, T. Nagashima, P. Newman, S. Pawson, G. Pitari, E. Rozanov, C. Schnadt, and T. G. Shepherd. Uncertainties and assessments of chemistry-climate models of the stratosphere, Atmos. Chem. Phys., 3, 1-27, 2003.

Grooß, J.-U., G. Günther, P. Konopka, R. Müller, D.S. McKenna, F. Stroh, B. Vogel, A. Engel, M. Müller, K. Hoppel, R. Bevilacqua, E. Richard, C.R. Webster, J.W. Elkins, D.F. Hurst, P.A. Romashkin and D.G. Baumgardner, Simulation of ozone depletion in spring 2000 with the Chemical Lagrangian Model of the Stratosphere (CLaMS), J. Geophys. Res., 2002.

Konopka, P., J.-U. Grooß, G. Günther, D.S. McKenna, R. Müller, J. W. Elkins, D. Fahey, and P. Popp, Weak impact of mixing on chlorine deactivation during SOLVE/THESEO2000: Lagrangian modeling (CLaMS) versus ER-2 in situ observations, J. Geophys. Res., 2003.

Konopka, P., H. Steinhorst, J.-U. Grooß, G. Günther, R. Müller, J. W. Elkins, H.-J. Joost, E. Richard, U. Schmidt, G. Toon and D. S. McKenna, Mixing and ozone loss in the 1999-2000 Arctic Vortex: Simulations with the three-dimensional Chemical Lagrangian Model of the Stratosphere (ClaMS), J. Geophys. Res., 2004.

Manzini, E., B. Steil, C. Brühl, M. A. Giorgetta and K. Krüger. A new interactive chemistry-climate model. II: Sensitivity of the middle atmosphere to ozone depletion and increase in greenhouse gases: Implications for recent stratospheric cooling. J. Geophys. Res., 108(D14), 4429, doi:10.1029/2002JD002977, 2003.

McKenna, D.S., P. Konopka, J.-U. Grooß, G. Günther, R. Müller, R. Spang, D. Offermann, and Y. Orsolini, A new Chemical Lagrangian Model of the Stratosphere (CLaMS): Part I Formulation of Advection and Mixing, J. Geophys. Res., 2001.

McKenna, D. S., J.-U. Grooß, G. Günther, P. Konopka, R. Müller, and G. Carver, A new Chemical Lagrangian Model of the Stratosphere (CLaMS): Part II Formulation of Chemistry Scheme and Initialisation, J. Geophys. Res., 2001.

Müller, R. and G. Günther, A generalized form of Lait's modified potential vorticity, J. Atmos. Sci., 60, pp. 2229-2237, 2003.

Steil, B., C. Brühl, E. Manzini, P.J. Crutzen, J. Lelieveld, P.J Rasch, E. Roeckner, K. Krüger, A new interactive chemistry climate model. I: Present day climatology and interannual variability of the middle atmosphere using the model and 9 years of HALOE/UARS data. J. Geophys. Res., 108(D9), 4290, doi:10.1029/2002JD002971, 2003.


## References:


Giorgetta, M. A. and L. Bengtsson, The potential role of the quasi-biennial oscillation in the stratosphere-troposphere exchange as found in water vapour in general circulation model experiments, J. Geophys. Res., 104, 6003-6019, 1999.

Hein, R., M. Dameris, C. Schnadt, C. Land, V. Grewe, I. Köhler, M. Ponater, R. Sausen, B. Steil, J. Landgraf, C. Brühl, Results of an interactively coupled atmospheric chemistry - general circulation model: Comparison with observations, Ann. Geophys., 19, 435-457, 2001.

Kirchner, I., G.L. Stenchikov, H.-F. Graf, A. Robock, and J.C. Antuna, Climate model simulation of winter warming and summer cooling following the 1991 Mount Pinatubo volcanic eruption, J. Geophys. Res., 104, 19039-19055, 1999.

Randel, W.J., F. Wu, and S.J. Oltmans, Interannual variability of stratospheric water vapor and correlations with tropical tropopause temperatures, J. Atmos. Sci., in press, 2004.

Ray, E., Moore, F. L., Elkins, J.W., Hurst, D. F., Romashkin, P. A., Dutton, G. S. and D. Fahey, Descent and Mixing in the 1999-2000 Northern Polar Vortex inferred from in-situ Tracer Measurements, J. Geophys. Res., 2002.

Rex, M., R.J. Salawitch, P. von der Gathen, N.R.P. Harris, M.P. Chipperfield, and B. Naujokat. Arctic ozone loss and climate change. Geophys.Res.Lett. 31, 4116, doi:10.1029/2003GL018844, 2004.

Steinbrecht, W., H. Claude, U. Köhler, and P. Winkler, Interannual changes of total ozone and northern hemisphere circulation patterns, Geophys. Res. Lett., 28, 1191-1194, 2001.